

Spin Relaxation Effects in Photochemically Induced Dynamic Nuclear Polarization Spectroscopy of Nuclei with Strongly Anisotropic Hyperfine Couplings

Ilya Kuprov,^{*,†} Timothy D. Craggs,[‡] Sophie E. Jackson,[‡] and P. J. Hore^{*,†}

Contribution from the Physical and Theoretical Chemistry Laboratory, Department of Chemistry, University of Oxford, South Parks Road, Oxford OX1 3QZ, U.K., and Chemistry Department, University of Cambridge, Lensfield Road, Cambridge CB2 1EW, U.K.

Received February 1, 2007; E-mail: ilya.kuprov@chem.ox.ac.uk; peter.hore@chem.ox.ac.uk

Abstract: We describe experimental results and theoretical models for nuclear and electron spin relaxation processes occurring during the evolution of ^{19}F -labeled geminate radical pairs on a nanosecond time scale. In magnetic fields of over 10 T, electron-nucleus dipolar cross-relaxation and longitudinal $\Delta\text{HFC}-\Delta g$ (hyperfine coupling anisotropy – g -tensor anisotropy) cross-correlation are shown to be negligibly slow. The dominant relaxation process is transverse $\Delta\text{HFC}-\Delta g$ cross-correlation, which is shown to lead to an inversion in the geminate ^{19}F chemically induced dynamic nuclear polarization (CIDNP) phase for sufficiently large rotational correlation times. This inversion has recently been observed experimentally and used as a probe of local mobility in partially denatured proteins (Khan, F.; et al. *J. Am. Chem. Soc.* **2006**, *128*, 10729–10737). The essential feature of the spin dynamics model employed here is the use of the complete spin state space and the complete relaxation superoperator. On the basis of the results reported, we recommend this approach for reliable treatment of magnetokinetic systems in which relaxation effects are important.

Introduction

Many fluorine-containing aromatic radicals and a number of phosphorus-centered radicals exhibit large and strongly anisotropic hyperfine couplings (HFC), sometimes exceeding 20 mT in strength.^{1,2} While large HFC anisotropy mostly generates unwanted complications in conventional electron paramagnetic resonance (EPR) spectroscopy, it can lead to qualitatively new phenomena in magnetochemical experiments, such as chemically induced dynamic nuclear polarization (CIDNP)^{3,4} and chemically induced dynamic electron polarization (CIDEP),^{4,5} which rely on a delicate interplay between spin dynamics and chemical kinetics.

Here we explore, both theoretically and experimentally, the effect of nuclear spin relaxation, cross-relaxation, and cross-correlation induced by the anisotropy of hyperfine and g -tensors on the geminate photo-CIDNP effect in fluorine-containing radicals. Apart from radicals containing ^{19}F and ^{31}P , the results are likely to be applicable to ^{13}C - and ^{15}N -containing species, as these nuclei can also have rather large isotropic and anisotropic HFCs in aromatic radicals, though usually not as

large as those of ^{19}F and ^{31}P .^{6,7} Given the proven utility of photo-CIDNP methods in protein folding research,⁸ the results will be particularly useful in the context of ^{13}C , ^{15}N , and ^{19}F photo-CIDNP spectroscopy of isotopically labeled proteins.^{9,10}

The starting point for the present work was provided by experimental observations^{9,10} of ^{19}F photo-CIDNP enhancements whose phases are opposite in sign to those predicted by the existing models,^{11–16} and which depend strongly on the molecular size and rotational correlation time. Below, we review reports of unexpected results from CIDNP and CIDEP experiments involving ^{19}F -containing radicals and verify that the existing models (based on the Overhauser effect^{11,17,18} or similar cross-relaxation and cross-correlation processes^{14–16,19}) are not consistent with phase inversions in measurements performed at high field (>10 T). We then perform a complete relaxation

- (6) Koleczak, U.; Rist, G.; Dietliker, K.; Wirz, J. *J. Am. Chem. Soc.* **1996**, *118*, 6477–6489.
- (7) Benn, R.; Dreeskamp, H. Z. *Phys. Chem.* **1976**, *101*, 11–23.
- (8) Kaptein, R.; Dijkstra, K.; Nicolay, K. *Nature* **1978**, *274*, 293–294.
- (9) Khan, F.; Kuprov, I.; Craggs, T. D.; Hore, P. J.; Jackson, S. E. *J. Am. Chem. Soc.* **2006**, *128*, 10729–10737.
- (10) Kuprov, I. D. Ph.D. thesis, University of Oxford, 2005, pp 1–154 (arXiv: physics/0604156).
- (11) Adrian, F. J. *Chem. Phys. Lett.* **1974**, *26*, 437–439.
- (12) Adrian, F. J. In ref 4, pp 77–105.
- (13) Kaptein, R. *Chem. Commun.* **1971**, 732–733.
- (14) Morozova, O. B.; Tsentlovich, Y. P.; Yurkovskaya, A. V.; Sagdeev, R. Z. *Chem. Phys. Lett.* **1995**, *246*, 499–505.
- (15) Tsentlovich, Y. P.; Frantsev, A. A.; Doktorov, A. B.; Yurkovskaya, A. V.; Sagdeev, R. Z. *J. Phys. Chem.* **1993**, *97*, 8900–8908.
- (16) Tsentlovich, Y. P.; Lopez, J. J.; Hore, P. J.; Sagdeev, R. Z. *Spectrochim. Acta A* **2002**, *58*, 2043–2050.
- (17) Overhauser, A. W. *Phys. Rev.* **1953**, *92*, 411–415.
- (18) Adrian, F. J.; Vyas, H. M.; Wan, J. K. S. *J. Chem. Phys.* **1976**, *65*, 1454–1461.
- (19) Adrian, F. J. In ref 4, pp 369–381.

[†] University of Oxford.

[‡] University of Cambridge.

- (1) Jockusch, S.; Turro, N. J. *J. Am. Chem. Soc.* **1998**, *120*, 11773–11777.
- (2) Vyshkova, M. M.; Beregovaya, I. V.; Vysotskii, V. P.; Shchegoleva, L. N.; Bagryanskii, V. A.; Molin, Y. N. *Dokl. Phys. Chem.* **2005**, *403*, 142–145.
- (3) Goetz, M. *Concepts Magn. Reson.* **1995**, *7*, 69–86.
- (4) Muus, L. T.; Atkins, P. W.; McLauchlan, K. A.; Pedersen, J. B. *Chemically induced magnetic polarization*; Proceedings of the NATO Advanced Study Institute, Sogesta, Urbino, Italy, April 17–30, 1977; D. Reidel: Dordrecht, Holland, 1977.
- (5) Hore, P. J.; Joslin, C. G.; McLauchlan, K. A. *Chem. Soc. Rev.* **1979**, *8*, 29–61.

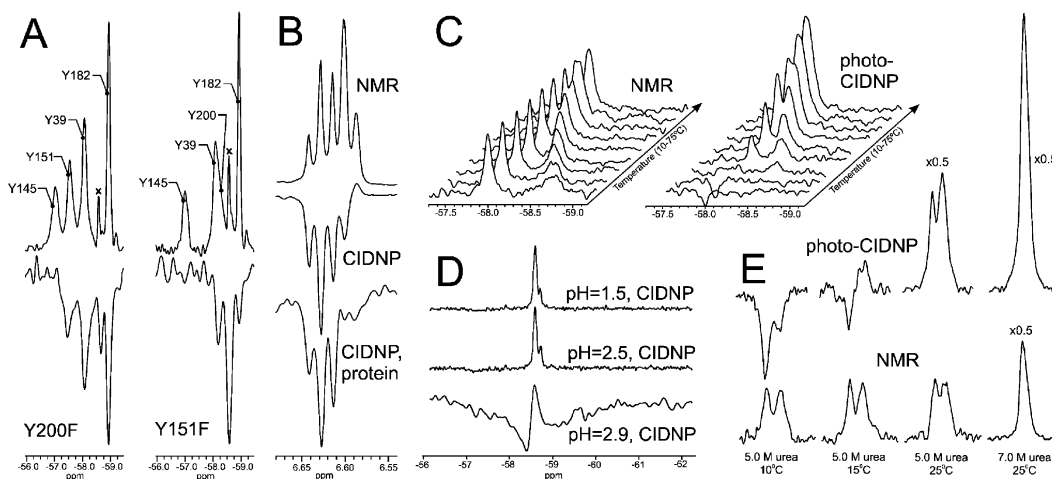


Figure 1. (A) ^{19}F NMR (top) and photo-CIDNP (bottom) spectra of Y200F and Y151F mutants of 3-fluorotyrosine-labeled green fluorescent protein. (B) Aromatic region of the ^1H NMR and photo-CIDNP spectra of 3-fluorotyrosine as the free amino acid (top and middle) and as an amino acid residue in the Trp-cage protein (bottom). (C) ^{19}F NMR and photo-CIDNP spectra of 3-fluorotyrosine-labeled Trp-cage protein as a function of temperature. The van't Hoff analysis of NMR intensities in the left panel results in $\Delta H^\circ = 7.6 \pm 1.6 \text{ kJ mol}^{-1}$, $\Delta S^\circ = 23 \pm 5 \text{ J K}^{-1} \text{ mol}^{-1}$, assuming a two-state chemical equilibrium, which we attribute to proline isomerization. (D) ^{19}F photo-CIDNP spectrum of 3-fluorotyrosine-labeled green fluorescent protein as a function of pH at 25 $^\circ\text{C}$. (E) ^{19}F photo-CIDNP spectrum of 3-fluorotyrosine-labeled Trp-cage protein as a function of denaturant concentration and temperature. (Panels A and D reproduced with permission from ref 9. Copyright 2006 American Chemical Society.)

analysis of our system, including all nonsecular and pseudo-secular terms, demonstrate that it successfully explains the experimental observations, and identify the relaxation pathways responsible.

Experimental and Computational Techniques

Our photo-CIDNP installations, as well as their *modus operandi*, are described in detail elsewhere.^{20,21} To achieve efficient illumination of strongly colored green fluorescent protein (GFP) solutions, a stepwise-tapered optical fiber was used in continuous-wave photo-CIDNP experiments, which permits efficient illumination of even very optically dense samples.²² The preparation of fluorine-labeled Trp-cage protein²³ is described in detail in ref 10, and that of fluorine-labeled GFP is described in ref 9.

For ^{19}F and ^1H photo-CIDNP experiments on 3-fluorotyrosine, D_2O solutions were used, each containing 4.0 mM 3-fluoro-DL-tyrosine (Lancaster), 0.2 mM flavin mononucleotide (FMN, Sigma), and 0–60% (by volume) of glycerol- d_8 (Cambridge Isotope Laboratories) at pH 7.0 (uncorrected for the deuterium isotope effect). For CIDNP experiments on fluorine-labeled GFP, its concentration in phosphate-buffered (50.0 mM, pH 7.2) D_2O was chosen to give an optical density of 1.0 at 514 nm, with 1.0 mM concentration of FMN. Photo-CIDNP experiments on Trp-cage were performed with 1.0 mM solutions in either pure D_2O or 5.0–7.0 M solutions of urea- d_4 in D_2O with 0.2 mM FMN as a photosensitizer.

The density functional theory (DFT) calculations were performed using the Gaussian03 program.²⁴ The equilibrium geometries were obtained from B3LYP/6-31++G(2d,2p) calculations performed in a combination of explicit (first solvation shell for polar groups) and implicit (PCM with UAKS topological atom model) water. Hyperfine and g -tensors were then computed for the resulting geometry on a GIAO B3LYP/EPR-III level of theory. This semi-explicit solvent approach yields hyperfine couplings in amino acid radicals that are in much better agreement with experimental results than calculations performed *in vacuo*.²⁵ All calculation logs can be found in the Supporting Information.

Ellipsoid plots of hyperfine tensors were generated using the `hfc_display` program, written in the Matlab 7.0 environment and listed in the Supporting Information. The program parses a single-point Gaussian log and draws every ellipsoid in the following way:

1. A unit sphere in a Cartesian space is scaled by $|A_{11}|$ in the X direction, $|A_{22}|$ in the Y direction, and $|A_{33}|$ in the Z direction, where A_{ii} are the eigenvalues of the HFC tensor and X , Y , and Z denote the principal axes of the tensor.

2. A set of three eigenaxes is drawn inside the ellipsoid with red for a positive eigenvalue and blue for a negative one.

3. The ellipsoid is translated to the position of the corresponding atom and rotated into the molecular frame.

Arguably, a more consistent way of representing the anisotropy of a symmetric second rank tensor would be to pull the ellipsoid inside-out through zero for negative eigenvalues so that the resulting plot looks like (and is in fact related to) a superposition of $Y_{2,m}(\theta, \varphi)$ spherical harmonics. It was found, however, that with this faithful representation the picture gets rather cluttered. Since the hyperfine tensor operates in a direct product of spin operator spaces, which fundamentally have no classical analogue, we believe that the details of its representation in a Cartesian space are a matter of convenience.

In deriving the relaxation superoperator for our model spin system, we make use of a convenient and powerful implementation of Bloch–Redfield–Wangsness (BRW) relaxation theory, based on rotation group theory and automated pattern matching. A detailed description of this approach, together with a few examples, can be found in our recent paper.²⁶ The specific program (written in Mathematica 5.2) we used to facilitate the relaxation theory treatment performed here may be found in the Supporting Information.

Survey of Experimental Observations

The starting point for the present work was the observation of ^{19}F photo-CIDNP effects in large fluorine-labeled molecules for which the phase of the net ^{19}F polarization was contrary to

(20) Kuprov, I.; Goetz, M.; Abbott, P. A.; Hore, P. J. *Rev. Sci. Instrum.* **2005**, *76* (084103), 1–7.

(21) Kuprov, I.; Hore, P. J. *J. Magn. Reson.* **2004**, *168*, 1–7.

(22) Kuprov, I.; Hore, P. J. *J. Magn. Reson.* **2004**, *171*, 171–175.

(23) Neidigh, J. W.; Fesinmeyer, R. M.; Andersen, N. H. *Nature Struct. Biol.* **2002**, *9*, 425–430.

(24) Frisch, M. J.; et al. *Gaussian 03*, Revision D.02; Gaussian, Inc.: Wallingford, CT, 2004.

(25) Adhikary, A.; Kumar, A.; Becker, D.; Sevilla, M. D. *J. Phys. Chem. B* **2006**, *110*, 24171–24180.

(26) Kuprov, I.; Wagner-Rundell, N.; Hore, P. J. *J. Magn. Reson.* **2007**, *184*, 196–206.

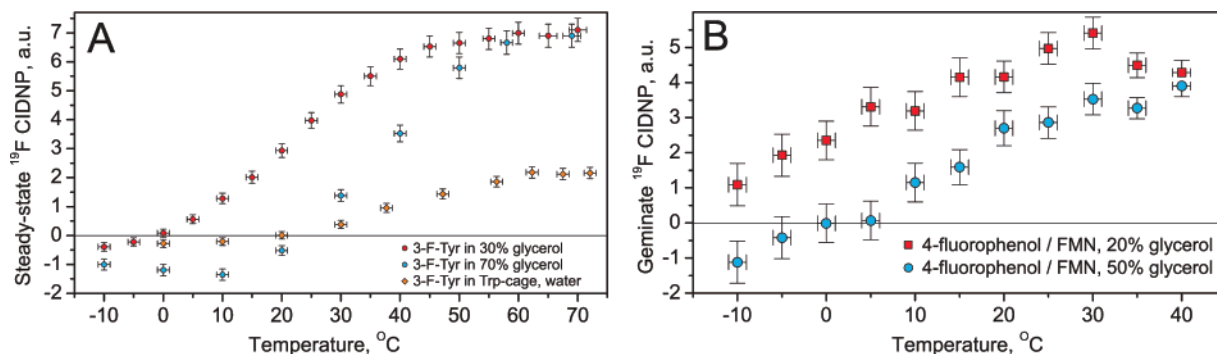


Figure 2. (A) Temperature dependence of the steady-state ^{19}F photo-CIDNP effect in water/glycerol solutions of 3-fluorotyrosine and in aqueous solution of 3-fluorotyrosine-labeled Trp-cage protein with FMN as the photosensitizer. (B) Temperature dependence of the geminate ^{19}F photo-CIDNP effect in water/glycerol solutions of 4-fluorophenol with FMN.

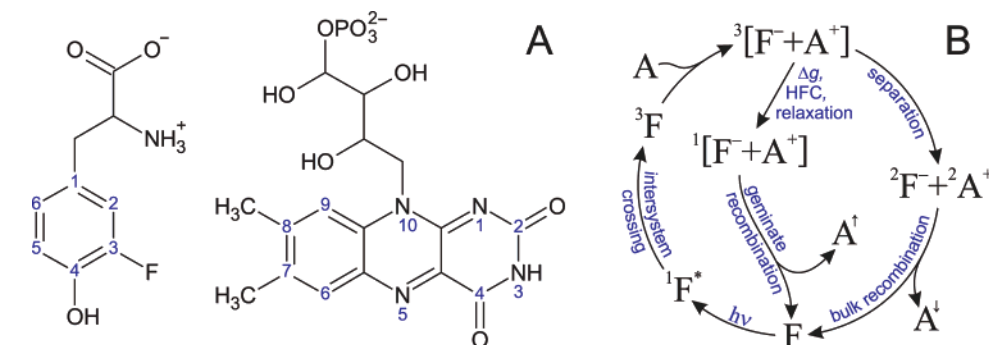


Figure 3. (A) Structures and atom numbering for 3-fluorotyrosine and flavin mononucleotide. (B) Schematic plot of the cyclic photochemical reaction chain responsible for the generation of the photo-CIDNP effect in FMN-sensitized systems.¹⁶

Kaptein's sign rule.¹³ The experimental results we reported earlier,^{9,10} and which we seek to explain here, are summarized in Figures 1 and 2. At a magnetic induction of 14.1 T (600 MHz ^1H NMR frequency), the following observations were made: (1) The ^{19}F photo-CIDNP effect in 3-fluorotyrosyl residues in two proteins (GFP⁹ and the TC5b variant of Trp-cage¹⁰) has a phase (emissive, Figure 1A,C) opposite to that of free 3-fluorotyrosine (absorptive) in aqueous solution.²¹ However, the ^1H photo-CIDNP effects have the same phase in a protein and the free amino acid (Figure 1B).¹⁰ (2) The sign of the ^{19}F photo-CIDNP effect changes from positive to negative for 3-fluorotyrosine and 4-fluorophenol when the solvent viscosity is increased (Figure 2A,B) by the addition of glycerol. The phase of the ^1H photo-CIDNP effect in the same system is unchanged.¹⁰ (3) For 3-fluorotyrosyl residues in GFP and Trp-cage, the sign of the ^{19}F photo-CIDNP effect changes from negative to positive when the protein is unfolded (Figures 1C–E and 2A). Once again, the ^1H CIDNP in the same residue is unaffected (not shown). (4) In all cases, it is the geminate CIDNP⁴ that changes sign. This is observed both directly (i.e., when the geminate effect is measured in a time-resolved CIDNP experiment) for 4-fluorophenol (Figure 2B) and indirectly (in a steady-state photo-CIDNP experiment) for 3-fluorotyrosine (Figure 2A). It has been shown that, due to fast spin relaxation of the ^{19}F nucleus in the radicals ($T_1 = 0.13 \mu\text{s}$), the steady-state ^{19}F CIDNP effect in 3-fluorotyrosine contains only the geminate contribution.²⁰ (5) The ^{19}F photo-CIDNP effect can have different signs for different 3-fluorotyrosyl residues in the same protein, depending on their respective mobilities (Figure 1C–E).^{9,10}

For the fluorine nucleus in the photoreactions of both 3-fluorotyrosine and 4-fluorophenol with FMN (Figure 3A), all four factors in Kaptein's sign rule for net nuclear polarization¹³ are positive:

$$\Gamma_{\text{net}}(i) = \mu \epsilon \text{sign}(\Delta g) \text{sign}(A_i) = \begin{cases} + & \text{absorptive} \\ - & \text{emissive} \end{cases};$$

$$\mu = \begin{cases} + & \text{triplet precursor} \\ - & \text{singlet precursor} \end{cases}; \quad (1)$$

$$\epsilon = \begin{cases} + & \text{recombination products} \\ - & \text{escape products} \end{cases}$$

In this equation, Δg is the difference between the g -values of the two radicals (fluorine-containing radical minus FMN radical) and A_i is the hyperfine coupling constant of the nucleus in question. The electron transfer in our systems is known to be initiated by a photoexcited triplet flavin molecule, and the recombination products are observed¹⁶ (Figure 3B), so both the μ and ϵ factors are positive. Together with the experimentally determined²⁷ or computed (see Table 1, below) g -values and hyperfine couplings, this results in the prediction of absorptive enhancement, which is indeed observed for the free 3-fluorotyrosine and 4-fluorophenol in aqueous solution.^{10,21}

To explain the experimentally observed phase inversion, without introducing additional sources of nuclear polarization, one of the factors in eq 1 must have a continuous dependence on temperature and/or solvent viscosity, possibly through another temperature- or viscosity-dependent parameter. Any change in the μ or ϵ factors should lead to a photo-CIDNP phase change for all nuclei simultaneously. This is not what is observed; nor

is it likely that μ could be negative, since the intersystem crossing in photoexcited flavins is known to be very fast.²⁸ Introducing an electronic structure perturbation sufficient to alter the sign of the ^{19}F hyperfine coupling or to shift the g -value requires either a large amount of energy (hyperfine coupling) or the introduction of strong spin-orbit coupling (g -factor). Neither is likely to be caused simply by raising the temperature by 15 °C (as shown in Figure 1E). The conclusion, therefore, is that some process or factor not included in Kaptein's rule is responsible. The chief suspect is spin relaxation, because the rotational correlation time is the obvious parameter that depends significantly on temperature, solvent viscosity, molecular size, and, for a protein, denaturation.

The unexpected behavior of the ^{19}F photo-CIDNP phase observed for small molecules appears to have a complex history, with attempted rationalizations mostly revolving around dipolar relaxation processes such as the Overhauser effect.^{11,14,18,19,29} A number of publications have reported unexpected contributions to the high-field CIDNP of Period II elements, manifested either at high viscosities or for very long-lived radicals in nonviscous solvents.^{30–32} Fluorine, with its large hyperfine coupling, has been cited as a classical example of Overhauser CIDNP, as proposed by Adrian in the 1970s.^{11,18,19,33,34} In a paper¹¹ analyzing earlier experimental work on p,p -difluorobenzyl,³⁵ Adrian reports detection of only ^{19}F polarization, whereas, according to the EPR hyperfine coupling data, ^1H polarization should also have been observed. Fluorine seemed to be special, and this was attributed to electron-nuclear cross-relaxation caused by the large HFC anisotropy of the fluorine nucleus.¹¹ A number of later works have also found or suspected an Overhauser contribution to CIDNP or CIDEF generation. For example, Borbat et al. argued that the inversion of a CIDEF multiplet effect from E/A to A/E is likely to be caused by cross-relaxation in high-viscosity solutions.³⁶

However, doubts have been cast on the Overhauser CIDNP idea: for example, Batchelor and Fischer³⁷ argued that earlier studies of photochemically generated CIDEF had incorrectly ascribed certain phenomena to cross-relaxation. They have demonstrated that, at a field of 4.7 T, cross-relaxation is negligibly slow and suggested instead that side reactions and fast solvent-dependent nuclear relaxation are responsible for the observed perturbation in the photo-CIDNP effect in the photochemical reaction of acetone and propan-2-ol. Also, Valyaev et al. ruled out an Overhauser mechanism as an explanation for certain unexpected CIDEF patterns, on the grounds that it is too slow under the conditions of their experiments.²⁹ What exactly caused those patterns is still unclear; as in the case of the acetone/propan-2-ol reaction,³⁷ secondary radical reactions might be responsible.

- (27) Landolt-Börnstein New Series: *Magnetic Properties of Free Radicals*; Springer-Verlag: Berlin, 1977; Group II, Vol. 1.
 (28) Climent, T.; Gonzalez-Luque, R.; Merchan, M.; Serrano-Andres, L. *J. Phys. Chem. A* **2006**, *110*, 13584–13590.
 (29) Valyaev, V. I.; Molin, Y. N.; Sagdeev, R. Z.; Hore, P. J.; McLauchlan, K. A.; Simpson, N. J. *K. Mol. Phys.* **1988**, *63*, 891–900.
 (30) Jent, F.; Paul, H. *Chem. Phys. Lett.* **1989**, *160*, 632–639.
 (31) Jent, F.; Paul, H.; McLauchlan, K. A.; Stevens, D. G. *Chem. Phys. Lett.* **1987**, *141*, 443–449.
 (32) Thomas, M. J.; Wagner, P. J.; Manion-Schilling, M. L.; Roth, H. D. *J. Am. Chem. Soc.* **1977**, *99*, 3842–3845.
 (33) Adrian, F. J. *Chem. Phys. Lett.* **1971**, *10*, 70–74.
 (34) Adrian, F. J.; Monchick, L. *J. Chem. Phys.* **1979**, *71*, 2600–2610.
 (35) Rakshys, J. W., Jr. *Tetrahedron Lett.* **1971**, 4745–4748.
 (36) Borbat, P. P.; Milov, A. D.; Molin, Y. N. *Pure Appl. Chem.* **1992**, *64*, 883–892.
 (37) Batchelor, S. N.; Fischer, H. *J. Phys. Chem.* **1996**, *100*, 556–564.

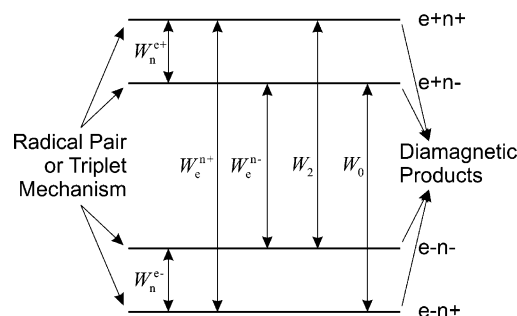


Figure 4. Energy levels and longitudinal relaxation transitions in an electron–nuclear two-spin system. Adapted, with modifications, from Adrian's treatment.¹⁸ See text for explanation of symbols.

The chief problem with Overhauser CIDNP and a large class of related longitudinal cross-relaxation and cross-correlation mechanisms is that, in high fields (14.1 T in our case), the calculations using BRW theory³⁸ and the models proposed by Adrian et al.^{11,18,19} and later Tsentlovich et al.^{14,15} all lead to values of the paramagnetic cross-relaxation and/or cross-correlation rates that are far too small to have any influence on the nanosecond time scale of geminate radical pair spin dynamics. A detailed analysis (which we present below) concludes that, while these mechanisms are clearly operational at lower fields and slower time scales,^{11,39} they do not explain our observations.

Analysis of Existing Models of Relaxation in CIDNP Systems

The first discussions of electron–nuclear dipolar cross-relaxation in the context of the CIDNP effect are attributed to Ward and Lawler^{40,41} and to Bargon and Fischer.^{42,43} Their description was subsequently adapted to the case of ^{19}F CIDNP by Adrian and co-workers.¹⁸ It considers only populations (neglecting coherences and cross-correlations) and includes all the pathways shown in Figure 4, amounting essentially to a classical four-level population dynamics model. It includes single-quantum transitions, corresponding to single spin flips (W_n and W_e terms), as well as double-quantum and zero-quantum transitions involving double spin flips (W_0 and W_2 terms). The transitions are assumed to be caused, in second-order time-dependent perturbation theory, by the stochastic modulation of the hyperfine coupling in one of the partners of the radical pair.

Our treatment (using the “BRW processor”²⁶) of Adrian's model resulted in the following expressions for the transition rates shown in Figure 4:

$$\begin{aligned}
 W_n^{e+} &= W_n^{e-} = \frac{\Delta_{\text{HFC}}^2}{480} [J(-\omega_n) + J(\omega_n)] \\
 W_e^{n+} &= W_e^{n-} = \frac{4\Delta_G^2 + \Delta_{\text{HFC}}^2}{480} [J(-\omega_e) + J(\omega_e)] \\
 W_2 &= \frac{\Delta_{\text{HFC}}^2}{120} [J(-\omega_e - \omega_n) + J(\omega_e + \omega_n)] \\
 W_0 &= \frac{\Delta_{\text{HFC}}^2}{720} [J(-\omega_e + \omega_n) + J(\omega_e - \omega_n)]
 \end{aligned}
 \tag{2}$$

- (38) Goldman, M. *J. Magn. Reson.* **2001**, *149*, 160–187.
 (39) Yamakage, Y.; Meng, Q.-X.; Maeda, K.; Azumi, T. *Chem. Phys. Lett.* **1993**, *204*, 411–414.
 (40) Lawler, R. G. *J. Am. Chem. Soc.* **1967**, *89*, 5519–5521.
 (41) Ward, H. R.; Lawler, R. G. *J. Am. Chem. Soc.* **1967**, *89*, 5518–5519.

Table 1. Calculated^a Hyperfine Couplings and *g*-Tensors for the 3-Fluorotyrosyl Radical and FMN Anion Radical

radical	atom	$(a_{xx} + a_{yy} + a_{zz})/3$, mT	$ 2a_{zz} - (a_{xx} + a_{yy}) $, mT	$ a_{xx} - a_{yy} $, mT	<i>g</i> -tensor parameters
3-fluorotyrosyl	C ⁽²⁾ -H	0.24	0.38	0.09	$g_{xx} = 2.0021$
	C ⁽³⁾ -F	1.25	14.16	0.44	$g_{yy} = 2.0051$
	C ⁽⁵⁾ -H	-0.52	1.01	0.16	$g_{zz} = 2.0073$
	C ⁽⁶⁾ -H	0.15	0.35	0.08	$g_{iso} = 2.0048$
	C ⁽¹⁾ -CH ₂ ^{-b}	0.41, 0.81	0.40, 0.40	0.03, 0.03	
flavin mononucleotide anion	N ⁽³⁾ -H	-0.02	0.20	0.03	$g_{xx} = 2.0019$
	C ⁽⁶⁾ -H	-0.30	0.48	0.04	$g_{yy} = 2.0041$
	C ⁽⁹⁾ -H	0.10	0.26	0.06	$g_{zz} = 2.0045$
	C ⁽⁷⁾ -CH ₃ ^b	-0.13, -0.13, -0.02	0.12, 0.12, 0.13	0.01, 0.01, 0.01	$g_{iso} = 2.0035$
	C ⁽⁸⁾ -CH ₃ ^b	0.64, 0.65, 0.02	0.21, 0.21, 0.17	0.01, 0.01, 0.00	
	N ⁽¹⁰⁾ -CH ₂ ^{-b}	0.20, 0.15	0.31, 0.30	0.01, 0.01	

^a Using GIAO DFT B3LYP 6-31++G(2d,2p)/EPR-III method in explicit + PCM water; see also Figure 5. ^b Conformationally mobile group; values given for the lowest energy conformation.

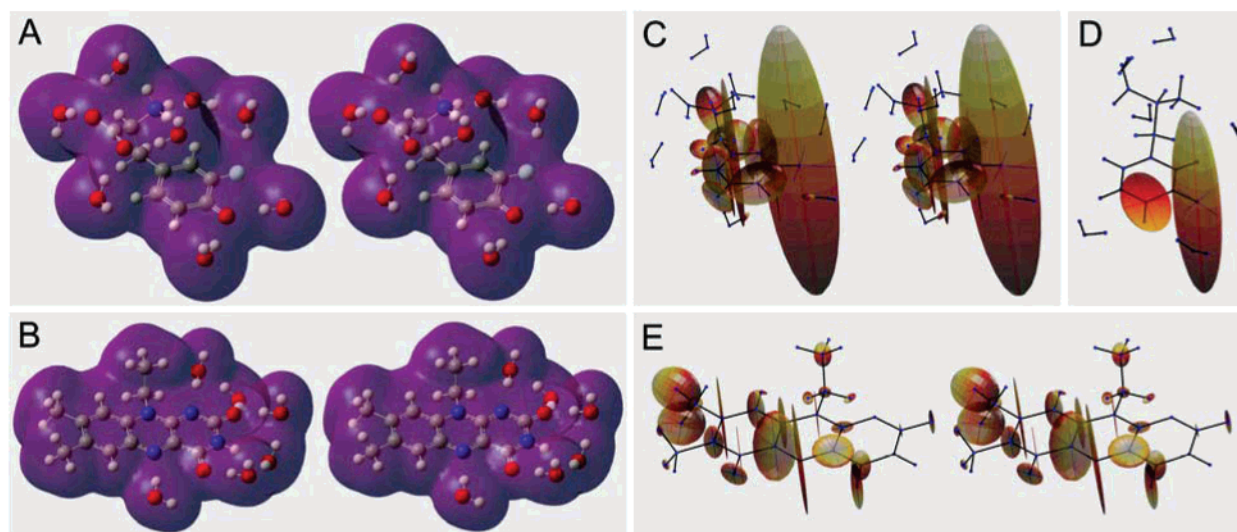


Figure 5. Stereoviews of (A) 3-fluorotyrosine and (B) flavin mononucleotide geometry obtained from B3LYP/6-31++G(2d,2p) calculations performed in a combination of explicit (first solvation shell for polar groups) and implicit (PCM with UAQS topological atom model) water. The purple surface is the solvation surface used in the PCM calculation. The ribityl side chain of the FMN has been truncated to an ethyl group. (C) Stereoview of an ellipsoid plot of hyperfine tensors in the 3-fluorotyrosyl radical. The hyperfine coupling tensors were computed using an EPR-III basis with the other parameters as above. (D) Relative orientations of the ¹⁹F hyperfine tensor and the *g*-tensor of the 3-fluorotyrosyl radical. The *g*-tensor was computed using the GIAO method in an EPR-III basis with the other parameters as above. The free electron *g*-factor was subtracted from the resulting *g*-tensor prior to plotting, to expose its anisotropy. (E) Stereoview of an ellipsoid plot of hyperfine tensors in flavin mononucleotide anion radical. The hyperfine coupling tensors were computed using an EPR-III basis with the other parameters as in panels A and B.

in which $J(\omega)$ is the spectral density function, ω_e and ω_n are Zeeman frequencies of electron and nucleus, respectively, and the hyperfine tensor and *g*-tensor anisotropy parameters are defined as

$$\begin{aligned}\Delta_T^2 &= Ax_T^2 + 3Rh_T^2 = 4(\mathbf{T}:\mathbf{T}); \\ Ax_T &= 2T_{ZZ} - (T_{XX} + T_{YY}); \\ Rh_T &= T_{XX} - T_{YY}\end{aligned}\quad (3)$$

where T refers to either the Zeeman or the hyperfine tensor and Ax and Rh refer to the axially and rhombicity of these tensors.

Even though it is often neglected, the spectral density function, strictly speaking, is not an even function of the frequency argument. We will omit this approximation and keep the

frequencies correctly signed. We also have an option here to improve the accuracy of eqs 2 slightly by also accounting for the *g*-hyperfine cross-correlation in the BRW theory treatment. We then get an electron relaxation rate differential between subensembles with different nuclear subspace configurations:

$$\begin{aligned}W_e^{n+} &= \frac{4\Delta_G^2 + \Delta_{\text{HFC}}^2 + 24X_{\text{G,HFC}}}{480} [J(-\omega_e) + J(\omega_e)] \\ W_e^{n-} &= \frac{4\Delta_G^2 + \Delta_{\text{HFC}}^2 - 24X_{\text{G,HFC}}}{480} [J(-\omega_e) + J(\omega_e)]\end{aligned}\quad (4)$$

The cross-correlation parameter $X_{\text{G,HFC}}$ can be written as

$$X_{\text{G,HFC}} = \left(\frac{Ax_{\text{HFC}}}{\sqrt{6}} \frac{Rh_{\text{HFC}}}{2} \right) \begin{pmatrix} \mathcal{D}_{0,0}^{(2)} & \mathcal{D}_{-2,0}^{(2)} + \mathcal{D}_{2,0}^{(2)} \\ \mathcal{D}_{0,-2}^{(2)} + \mathcal{D}_{0,2}^{(2)} & \mathcal{D}_{-2,-2}^{(2)} + \mathcal{D}_{-2,2}^{(2)} + \mathcal{D}_{2,-2}^{(2)} + \mathcal{D}_{2,2}^{(2)} \end{pmatrix} \quad (5)$$

where the Wigner functions $\mathcal{D}_{m,k}^{(2)}(\alpha, \beta, \gamma)$ depend on the three

(42) Bargon, J.; Fischer, H. *Z. Naturforsch. A: Astrophys., Phys. Phys. Chem.* **1967**, *22*, 1556–1562.

(43) Bargon, J.; Fischer, H.; Johnsen, U. *Z. Naturforsch. A: Astrophys., Phys. Phys. Chem.* **1967**, *22*, 1551–1555.

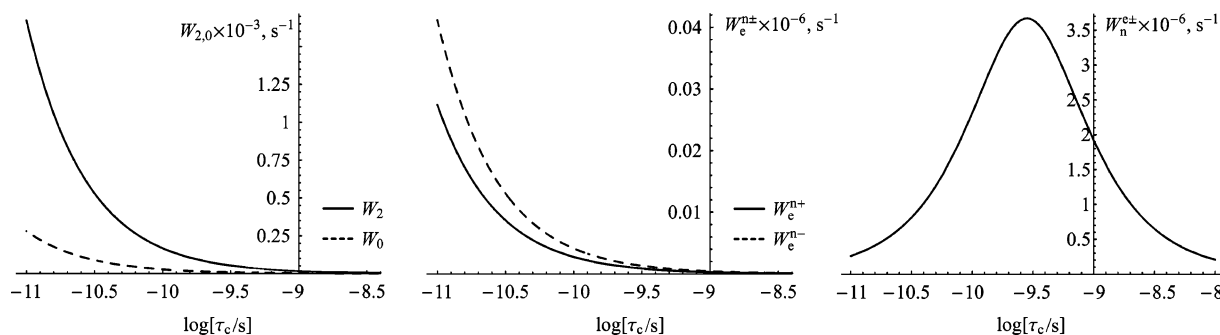


Figure 6. Rotational correlation-time dependence of the rates of relaxation transitions (eqs 2 and 4) for the 3-fluorotyrosine radical at 14.1 T magnetic field using the computed values of hyperfine and g -tensor anisotropy.

Euler angles that link the eigenframes of the Zeeman and hyperfine tensors. The $X_{G,HFC}$ parameter in the form given in eq 5 deserves a special mention. It is the most general form of the cross-correlation parameter for any pairwise cross-correlation between any second-rank spin interaction tensors. In the axial case it simplifies to the familiar expression^{44,45}

$$X_{G,HFC} = \frac{A_{xG} A_{xHFC}}{12} [3 \cos^2 \beta - 1] \quad (6)$$

in which β refers to the angle between the main axes of the two tensors. Equation 6 is frequently encountered in the context of pairwise cross-correlations in NMR spectroscopy.^{45,46} We have yet to find the full form of eq 5 in the literature; it may become useful once the accuracy of cross-correlation experiments in NMR improves beyond the axial approximation, e.g., for cross-correlation of rhombic chemical shift tensors.²⁶

In the case of the 3-fluorotyrosyl radical, all of the required interaction parameters may be computed (Table 1, Figure 5, and Gaussian03²⁴ logs in the Supporting Information). The resulting values (in squared angular frequency units at 14.1 T) are $\Delta_G^2 = 1.26 \times 10^{20}$, $\Delta_{HFC}^2 = 6.24 \times 10^{18}$, and $X_{G,HFC} = -4.26 \times 10^{18}$. In the isotropic tumbling approximation, i.e., with

$$J(\omega) = \frac{\tau_c}{(1 + \tau_c^2 \omega^2)} + \frac{i\omega \tau_c^2}{(1 + \tau_c^2 \omega^2)} \quad (7)$$

(where τ_c is the rotational correlation time), the transition rates in eqs 2 and 4 for the case of the 3-fluorotyrosyl radical in a 14.1 T magnetic field are plotted against the correlation time in Figure 6. It is obvious that, across the entire range of experimentally available correlation times (10 ps–10 ns), the electron-nucleus cross-relaxation rates W_0 and W_2 are too small to exert any influence whatsoever on the nanosecond to microsecond time scale photo-CIDNP spin dynamics a consequence of having the square of the electron Larmor frequency in the spectral density denominators in eqs 2. Although the nuclear relaxation rate W_n may become large enough to manifest itself in secondary reactions ($3.6 \times 10^6 \text{ s}^{-1}$ for $\tau_c = 0.3 \text{ ns}$, Figure 6), it does not lead to spin selection, since $W_n^{e+} = W_n^{e-}$. Thus, at the field of 14.1 T, no nuclear spin selection occurs as a result of the relaxation transitions shown in Figure 4.

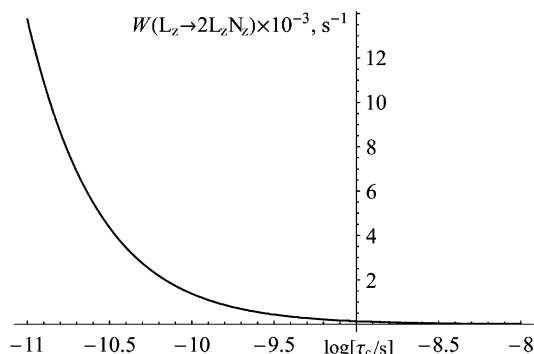


Figure 7. Rotational correlation-time dependence of the longitudinal $\Delta HFC - \Delta g$ cross-correlation rate $W(L_Z \leftrightarrow 2L_Z N_Z)$ for the 3-fluorotyrosine radical at 14.1 T magnetic field using the computed values of hyperfine and g -tensor anisotropy.

Tsentulovich and co-workers have extended Adrian's description of Overhauser CIDNP^{14,15} by explicitly including longitudinal multi-spin orders in the relaxation treatment, thereby expanding the number of spin states that are properly accounted for in the model. As applied to the above model of 3-fluorotyrosine radical, this refinement amounts to including the longitudinal two-spin order $2L_Z N_Z$ (here and below, L and S denote electron spin operators and N the nuclear ones) in the description. Within BRW theory, we obtained the following rate for the $L_Z \leftrightarrow 2L_Z N_Z$ transition:

$$W(L_Z \leftrightarrow 2L_Z N_Z) = -\frac{X_{G,HFC}}{10} [J(-\omega_e) + J(\omega_e)] \quad (8)$$

It is obvious from Figure 7 that, at 600 MHz, this extended model suffers from the same problem as Adrian's model: actual calculations lead to values of the rates that are far too small to have any influence on the photo-CIDNP time scale.

On the positive side, it had been proven very convincingly^{18,39} that, at *low magnetic field* (<20 MHz ¹H frequency), the Overhauser mechanism does contribute to the generation of photo-CIDNP polarization of fluorine nuclei. This is correctly predicted by eqs 2 and 4 above, because the spectral density denominators at 20 MHz are no longer small. At higher fields, the Overhauser effect can still be detected if the lifetime of the intermediate radicals is prolonged beyond several tens of microseconds, as happens in the system reported by Roth et al.³² However, this is not the case here (at 600 MHz).

In summary, it is well established that, at low field, the electron does cross-relax with the nucleus during the lifetime

(44) Goldman, M. *J. Magn. Reson.* **1984**, *60*, 437–452.

(45) Kumar, A.; Grace, R. C. R.; Madhu, P. K. *Prog. Nucl. Magn. Reson. Spectrosc.* **2000**, *37*, 191–319.

(46) Kumar, A.; Madhu, P. K. *Concepts Magn. Reson.* **1996**, *8*, 139–160.

of the radical pair, provided the HFC anisotropy is large enough. Why the same thing appears to happen at high fields is less clear – the simple calculation outlined above demonstrates that, in a 600 MHz magnetic field, all the longitudinal relaxation, longitudinal cross-relaxation, and longitudinal cross-correlation rates become too small and cannot, at least according to the current models, exert an influence on the nanosecond to microsecond time scale of photo-CIDNP generation. Below we report a detailed theoretical investigation, which identifies the mechanism responsible.

Complete Relaxation Superoperator Model Results and Discussion

It is apparent from the above discussion that spin dynamics models that include only a selection of the possible spin orders and relaxation mechanisms fail to predict the experimentally observed behavior. We therefore decided to adopt a brute force approach, namely to compute a *complete* (4096 elements) symbolic relaxation superoperator for the three-spin system (two electrons and a nucleus) under consideration using our recently developed symbolic processing software,²⁶ and then to perform the spin dynamics calculation in the complete operator space, including transverse magnetization and other coherence operators. If a dependence of the high-field geminate ¹⁹F photo-CIDNP on the correlation time is predicted, one can then try to identify the relaxation pathway(s) responsible.

An essential feature of fluorinated aromatic radicals is the large and strongly anisotropic ¹⁹F hyperfine coupling. The isotropic HFCs may reach 5 mT in radical cations¹⁰ and over 20 mT in nonplanar radical anions² (a typical hyperfine coupling to an aromatic proton is ≤ 0.7 mT). The ¹⁹F hyperfine anisotropy is also very large, e.g., 24.2 mT in the 4-fluorophenoxyl radical.¹⁰ Rotational modulation of hyperfine interactions, along with rotational modulation of the anisotropic Zeeman interaction, is the primary relaxation mechanism in aromatic radicals in liquids;⁴⁷ furthermore, the relaxation rate is quadratic in HFC anisotropy. We should therefore expect nuclear spin relaxation to be very fast, at least for some correlation times, and expect relaxation processes to play a major role in ¹⁹F CIDNP formation. Because the applied magnetic field is very high (14.1 T), we should also include the Zeeman interaction anisotropy and Zeeman–HFC cross-correlation, since the Zeeman mechanism is quadratic in the field and rapidly becomes important as one moves to higher fields.

A number of assumptions need to be made before we can proceed with the modeling and relaxation theory treatment of spin dynamics in 3-fluorotyrosine/FMN radical pairs. Because the ¹⁹F hyperfine coupling is significantly stronger than any other HFC in either 3-fluorotyrosine cation or FMN anion (see Table 1 and Figure 5), we will use a single-nucleus approximation (i.e., we treat a system comprising two electron spins and the ¹⁹F spin). Since the applied field is strong, the nonsecular parts of the isotropic Zeeman and isotropic hyperfine interactions will be neglected. We will also neglect the anisotropy of the nuclear shielding tensor: at 14.1 T, it is of the order of kilohertz and is completely swamped by the much stronger Zeeman and hyperfine interactions, in both zero-order and relaxation theory contributions. The inter-electron dipolar and exchange interactions will also be neglected for two reasons. First, the two radicals are assumed to be sufficiently far apart on average that the effect

of these interactions is small.⁴ Second, we are seeking, in this treatment, to explain a nucleus-centered phenomenon, for which these inter-electron couplings cannot be responsible. Finally, we shall neglect the coupling between the spatial and spin degrees of freedom (normally caused by the above-mentioned dipolar and exchange interactions) by using a spin-independent re-encounter probability distribution, which will be combined with a separately computed spin evolution trajectory.

With the assumptions outlined above, the spin Hamiltonian of a single-nucleus radical pair, separated into the “strong” time-independent part, \hat{H}_0 , and the “weak” stochastic part, $\hat{H}_1(t)$, has the following form:

$$\begin{aligned} \hat{H}_0 &= \omega_L \hat{L}_Z + \omega_S \hat{S}_Z + \omega_n \hat{N}_Z + a \hat{L}_Z \hat{N}_Z \\ \hat{H}_1(t) &= \hat{R}_{\text{mol}}^{(1)} \hat{R}_{\text{pos}}^{\text{HFC}} (\hat{L} \cdot \mathbf{A} \cdot \hat{N}) + \hat{R}_{\text{mol}}^{(1)} \hat{R}_{\text{pos}}^{\text{Z1}} (\hat{L} \cdot \mathbf{Z}_1 \cdot \hat{B}) + \\ &\quad \hat{R}_{\text{mol}}^{(2)} \hat{R}_{\text{pos}}^{\text{Z2}} (\hat{S} \cdot \mathbf{Z}_2 \cdot \hat{B}) \end{aligned} \quad (9)$$

where ω_L , ω_S , and ω_n are the Larmor frequencies of the two electrons and the nucleus, a is the isotropic hyperfine coupling constant, \hat{R}_{pos} are the static “positioning” rotations that take the interaction tensors (\mathbf{A} for hyperfine and $\mathbf{Z}_{1,2}$ for Zeeman) from their eigenframes to the molecular frame, and $\hat{R}_{\text{mol}}^{(1,2)}$ are the time-dependent overall rotations of the two radicals, together with the interactions defined within them. Translating the operators and rotations in the perturbation part into irreducible spherical tensor notation,^{26,48,49} we get

$$\begin{aligned} \hat{H}_1(t) &= \sum_{k,m=-2}^2 \mathcal{M}_{k,m}^{(2)}(t) [\hat{T}_{2,k}^{(\text{HFC})} \Phi_m^{(\text{HFC})} + \hat{T}_{2,k}^{(\text{Z1})} \Phi_m^{(\text{Z1})}] + \\ &\quad \sum_{k,m=-2}^2 \mathcal{N}_{k,m}^{(2)}(t) [\hat{T}_{2,k}^{(\text{Z2})} \Phi_m^{(\text{Z2})}] \end{aligned} \quad (10)$$

$$\begin{aligned} \Phi_m^{(\text{A})} &= \frac{A_{\text{XX}} - A_{\text{YY}}}{2} (\mathcal{D}_{m,-2}^{(2)} + \mathcal{D}_{m,2}^{(2)}) + \\ &\quad \frac{2A_{\text{ZZ}} - (A_{\text{XX}} + A_{\text{YY}})}{\sqrt{6}} \mathcal{D}_{m,0}^{(2)} \end{aligned} \quad (11)$$

where $\mathcal{M}_{k,m}^{(2)}(t)$ and $\mathcal{N}_{k,m}^{(2)}(t)$ are Wigner functions defining the laboratory frame orientation of the first and second radicals, respectively, and $\Phi_m^{(\text{HFC})}$, $\Phi_m^{(\text{Z1})}$, and $\Phi_m^{(\text{Z2})}$ are linear combinations of Wigner functions $\mathcal{D}_{m,k}^{(2)}$ defining the orientations of the hyperfine and two Zeeman tensors (eigenvalues A_{XX} , A_{YY} , A_{ZZ} with $A = \text{Z1, Z2, or HFC}$) in their respective molecular frames.

For the rotational correlation functions of both radicals, we will make the isotropic tumbling approximation; therefore, the correlation functions are exponentials:

$$\begin{aligned} \overline{\mathcal{M}_{a,b}^{(2)}(t) \mathcal{M}_{c,d}^{(2)*}(t + \tau)} &= \frac{\delta_{a,c} \delta_{b,d}}{5} e^{-\tau/\tau_c^{(1)}} \\ \overline{\mathcal{N}_{a,b}^{(2)}(t) \mathcal{N}_{c,d}^{(2)*}(t + \tau)} &= \frac{\delta_{a,c} \delta_{b,d}}{5} e^{-\tau/\tau_c^{(2)}} \end{aligned} \quad (12)$$

where the overbar denotes ensemble averaging and $\tau_c^{(1,2)}$ are the rotational correlation times of the two radicals. Because the radicals are assumed to have moved sufficiently far apart to

(47) Kowalewski, J.; Mäler, L. *Nuclear spin relaxation in liquids: theory, experiments, and applications*; Taylor & Francis: London, 2006; p 252.
(48) Freed, J. H.; Fraenkel, G. K. *J. Chem. Phys.* **1963**, *39*, 326–348.

Table 2. Self-Relaxation Rates of \hat{H}_0 Eigenstates^a

spin order	\hat{H}_0 eigenvalue	dipolar part	Zeeman part	cross-correlation part
L_Z	0	$-(\Delta_{\text{HFC}}^2/36)J(\omega_L)$	$-(\Delta_{\text{G1}}^2/30)J(\omega_L)$	0
N_Z	0	$-(\Delta_{\text{HFC}}^2/36)[3J(\omega_N) + 7J(\omega_L)]$	0	0
$L_Z N_Z$	0	$-(\Delta_{\text{HFC}}^2/120)[J(\omega_N) + J(\omega_L)]$	$-(\Delta_{\text{G1}}^2/30)J(\omega_L)$	0
$N_{\pm} + 2N_{\pm} L_Z$	$\pm\omega_N \pm a/2$	$-(\Delta_{\text{HFC}}^2/720)[4J(0) + 3J(\omega_N) + 10J(\omega_L)]$	$-(\Delta_{\text{G1}}^2/60)J(\omega_L)$	0
$N_{\pm} - 2N_{\pm} L_Z$	$\pm\omega_N \mp a/2$	$-(\Delta_{\text{HFC}}^2/720)[4J(0) + 3J(\omega_N) + 10J(\omega_L)]$	$-(\Delta_{\text{G1}}^2/60)J(\omega_L)$	0
$L_{\pm} + 2L_{\pm} N_Z$	$\pm\omega_L \pm a/2$	$-(\Delta_{\text{HFC}}^2/720)[4J(0) + 3J(\omega_N) + 10J(\omega_L)]$	$-(\Delta_{\text{G1}}^2/180)[4J(0) + 3J(\omega_L)]$	$-(X_{\text{G1,HFC}}/30)[4J(0) + 3J(\omega_L)]$
$L_{\pm} - 2L_{\pm} N_Z$	$\pm\omega_L \mp a/2$	$-(\Delta_{\text{HFC}}^2/720)[4J(0) + 3J(\omega_N) + 10J(\omega_L)]$	$-(\Delta_{\text{G1}}^2/180)[4J(0) + 3J(\omega_L)]$	$+(X_{\text{G1,HFC}}/30)[4J(0) + 3J(\omega_L)]$
$L_{\pm} N_{\pm}$	$\pm\omega_L \pm \omega_N$	$-(\Delta_{\text{HFC}}^2/240)[J(\omega_N) + 5J(\omega_L)]$	$-(\Delta_{\text{G1}}^2/180)[4J(0) + 3J(\omega_L)]$	0
$L_{\pm} N_{\mp}$	$\pm\omega_L \mp \omega_N$	$-(\Delta_{\text{HFC}}^2/720)[3J(\omega_N) + 5J(\omega_L)]$	$-(\Delta_{\text{G1}}^2/180)[4J(0) + 3J(\omega_L)]$	0

^a See text for the list of assumptions and approximations used in deriving these expressions.

Table 3. Secular and Weakly Nonsecular^a Cross-Relaxation Rates between \hat{H}_0 Eigenstates

source spin order	destination spin order	absolute \hat{H}_0 eigenvalue difference	dipolar part	Zeeman part	cross-correlation part
L_Z	N_Z	0	$-(\Delta_{\text{HFC}}^2/72)J(\omega_L)$	0	0
	$L_Z N_Z$	0	0	0	$-(X_{\text{G1,HFC}}/5)J(\omega_L)$
N_Z	L_Z	0	$-(\Delta_{\text{HFC}}^2/72)J(\omega_L)$	0	0
$L_Z N_Z$	L_Z	0	0	0	$-(X_{\text{G1,HFC}}/5)J(\omega_L)$
$N_{\pm} + 2N_{\pm} L_Z$	$N_{\pm} - 2N_{\pm} L_Z$	a	$-(\Delta_{\text{HFC}}^2/240)J(\omega_L)$	$-(\Delta_{\text{G1}}^2/60)J(\omega_L)$	0
$N_{\pm} - 2N_{\pm} L_Z$	$N_{\pm} + 2N_{\pm} L_Z$	a	$-(\Delta_{\text{HFC}}^2/240)J(\omega_L)$	$+(\Delta_{\text{G1}}^2/60)J(\omega_L)$	0
$L_{\pm} - 2L_{\pm} N_Z$	$L_{\pm} + 2L_{\pm} N_Z$	a	$-(\Delta_{\text{HFC}}^2/240)J(\omega_N)$	0	0
$L_{\pm} + 2L_{\pm} N_Z$	$L_{\pm} - 2L_{\pm} N_Z$	a	$-(\Delta_{\text{HFC}}^2/240)J(\omega_N)$	0	0

^a The definitions of secular and weakly nonsecular cross-relaxation rates and the list of assumptions and approximations used in deriving these expressions are given in the main text.

behave independently, the rotational functions $\mathcal{M}_{m,k}^{(2)}(t)$ are independent of $\mathcal{N}_{m,k}^{(2)}(t)$, meaning that all ensemble correlation functions between the two sets are zero:

$$\overline{\mathcal{M}_{m,k}^{(2)}(t) \mathcal{N}_{m',k'}^{(2)}(t + \tau)} = 0 \quad (13)$$

Because the g -tensor and the hyperfine coupling tensor in the first radical share the same set of overall rotation functions $\mathcal{M}_{m,k}^{(2)}(t)$ in the Hamiltonian (eq 10), the cross-correlation between the anisotropies of these tensors will be correctly accounted for.²⁶ As we shall see below, it is this cross-correlation that causes the CIDNP phase to invert for long correlation times.

Submitting the Hamiltonian (eq 10) with correlation functions (eqs 12 and 13) into the BRW theory processor described elsewhere²⁶ yields the relaxation and cross-relaxation rates reported in Tables 2 and 3. The program gives the general result, which includes the dynamic frequency shift and all nonsecular components. For example, the self-relaxation rate of the $L_{+} + 2L_{+} N_Z$ eigenstate of \hat{H}_0 is

$$R_{L_{+} + 2L_{+} N_Z} = -\frac{\Delta_{\text{G1}}^2}{120} [J(\omega_L - a/2) + J(-\omega_L - a/2)] - \frac{\Delta_{\text{HFC}}^2}{1440} \left[\begin{aligned} &8J(0) + 6J(-\omega_N - a/2) + 3J(-\omega_L - a/2) + \\ &12J(-\omega_L - \omega_N) + 3J(\omega_L - a/2) + 2J(-\omega_L + \omega_N) \end{aligned} \right] - \frac{X_{\text{G1,HFC}}}{20} [J(\omega_L - a/2) + J(-\omega_L - a/2)] \quad (14)$$

where $L_{\pm} = L_X \pm iL_Y$ and other symbols were defined above. So far as BRW theory goes, eq 14 is exact. However, this high level of detail is rarely necessary, and we can make considerable simplifications by observing that, in our case, $a/2 \ll \omega_N \ll \omega_{L,S}$ and neglecting the dynamic frequency shifts, i.e., setting $J(-\omega) = J(\omega)$. With that in place, the result for $L_{+} + 2L_{+} N_Z$ simplifies to

$$R_{L_{+} + 2L_{+} N_Z} = -\frac{\Delta_{\text{HFC}}^2}{720} [4J(0) + 3J(\omega_N) + 10J(\omega_L)] - \frac{\Delta_{\text{G1}}^2}{180} [4J(0) + 3J(\omega_L)] - \frac{X_{\text{G1,HFC}}}{30} [4J(0) + 3J(\omega_L)] \quad (15)$$

and it is expressions of this type that we chose to tabulate (Tables 2 and 3). The relaxation of the other radical (flavin mononucleotide anion) is assumed to be dominated by the g -tensor anisotropy term, since there are no large hyperfine anisotropies (Table 1). The corresponding rates may be obtained from Table 2 by setting $\Delta_{\text{HFC}}^2 = 0$, $X_{\text{G1,HFC}} = 0$ and replacing Δ_{G1}^2 with Δ_{G2}^2 .

The resulting relaxation superoperator contains three classes of transitions. The ‘‘secular’’ ones, such as the $L_Z \rightarrow N_Z$ electron-nuclear cross-relaxation, occur between the eigenstates of \hat{H}_0 with zero frequency separation (the eigenvalues are given in Table 2). We certainly need to retain those. The ‘‘weakly nonsecular’’ class comprises those transitions which occur over relatively narrow frequency gaps (e.g., $\Delta\omega = a$ or $\Delta\omega = \omega_N$),

(49) Sanctuary, B. C.; Halstead, T. K. *Adv. Magn. Reson.* **1990**, *15*, 79–161.

such as $N_{\pm} + 2N_{\pm}L_Z \rightarrow N_{\pm} - 2N_{\pm}L_Z$. Because the relaxation events in our system are expected to operate on the microsecond to nanosecond time scale, such frequency gaps are small enough for these relaxation pathways to be manifested, so we keep them as well. The “strongly nonsecular” class contains transitions which occur over frequency differences of the order of $\Delta\omega = \omega_{L,S}$. These transitions are firmly nonsecular in the system under study and are likely to be unimportant. Table 3, therefore, contains only the secular and weakly nonsecular terms of the relaxation superoperator. The simulation was still done with the full unsimplified relaxation matrix (the Mathematica program included in the Supporting Information will print the nonsecular terms on demand).

With the relaxation superoperator generated as described above, we can compute the spin dynamics in the 3-fluorotyrosine/FMN system by brute force, by numerically propagating the initial electron-only triplet state, all the way to complete magnetization equilibration, i.e., to 5 times the reciprocal of the slowest relaxation rate. During the actual calculations, care must be taken not to exceed the applicability range of the BRW theory, which is roughly $\tau_c \ll \min\{R_i^{-1}\}$, where R_i are the computed relaxation rates. This criterion is likely to have an ample safety margin,^{38,50} and it is generally believed that the theory remains quantitatively correct until $\tau_c \approx \max\{R_i^{-1}\}$, and there are indications that it may be reliable far beyond that point.⁵¹

For the radical re-encounter probability distribution, we chose the function proposed by Noyes,^{52,53} which is known to reproduce experimental findings in a large variety of systems. In practice, it is convenient to use a mathematically equivalent formulation, suggested by Adrian,¹² which is parametrized in a more transparent way:

$$f(t) = \frac{R_o(R_0 - R_o)}{R_0} \sqrt{\frac{1}{4\pi Dt^3}} \exp\left[-\frac{(R_0 - R_o)^2}{4Dt}\right] \quad (16)$$

where D is the relative diffusion coefficient of the two radicals, R_0 is the initial radical separation (assumed to be 10 Å), and R_o is the separation at which the radicals recombine (assumed to be 5 Å). [The result of the simulation is insensitive to R_0 and R_o over a wide range of their values, since on the time scale of the singlet–triplet interconversion the exponential in eq 16 almost instantaneously reaches a value of unity, leaving just the $t^{-3/2}$ term with a constant multiplier.] We use Kaptein’s assumptions (small singlet–triplet transition probability compared to the singlet recombination rate, spin-independent re-encounter statistics)^{54,55} regarding the treatment of repetitive encounters. The recombination only occurs from the singlet radical pair state in FMN-sensitized photo-CIDNP systems;¹⁶ therefore, the overall singlet yield Φ_S and the residual nuclear magnetization $\langle N_Z \rangle$ are calculated, up to a constant factor, as integrated traces of the density operator $\hat{\rho}(t)$ with the electron singlet projector \hat{P}_S and the $\hat{P}_S \hat{N}_Z$ spin order, respectively:

$$\begin{aligned} \Phi_S &= \int_0^{\infty} \text{Tr}[\hat{P}_S \hat{\rho}(t)] f(t) dt; \\ \langle N_Z \rangle &= \int_0^{\infty} \text{Tr}[\hat{P}_S \hat{N}_Z \hat{\rho}(t)] f(t) dt \end{aligned} \quad (17)$$

Computing the geminate ¹⁹F photo-CIDNP for the 3-fluorotyrosine/FMN system with the static Hamiltonian \hat{H}_0 from eq 9, and the complete relaxation matrix (Tables 2 and 3) obtained from the dynamic Hamiltonian in eq 10 with computed (Table 1) spin system parameters using the re-encounter probability model in eq 16 (the program source code is included in the Supporting Information) results in the correlation-time dependence shown in Figure 8. The computed geminate ¹⁹F photo-CIDNP effect (Figure 8, blue surface) goes negative as the correlation time of the fluorine-containing radical is increased. In other words, the model succeeds in predicting the experimental results in Figures 1 and 2. The zero crossing for the ¹⁹F photo-CIDNP effect is predicted to occur around $\tau_c = 0.5$ ns, in agreement with the GFP⁹ and Trp-cage (Figure 1E) data. The direction of the correlation-time dependence is determined by the sign of the $X_{G1,HFC}$ function, which is negative in the 3-fluorotyrosyl radical. Figure 8 also shows the other two cases, namely when $X_{G1,HFC}$ is positive and zero. With positive $X_{G1,HFC}$ of identical magnitude (e.g., in a radical with a different relative orientation of hyperfine and g -tensors), there is constructive interference between the RPM-generated and relaxation-generated geminate photo-CIDNP effect (black surface). When either the HFC or the g -tensor is isotropic, the CIDNP effect monotonically falls to zero, due to nonselective decoherence (green surface), when the correlation times are increased. This type of behavior is characteristic of a cross-correlated relaxation process.

It thus appears that, after all the relaxation pathways have been taken into account, the correlation-time dependence of the high-field geminate ¹⁹F photo-CIDNP effect may be explained, completely *ab initio* and without adjustable parameters. The important question now is which particular relaxation pathway is responsible for this phenomenon. A systematic inspection of the effect of each relaxation route given in Tables 2 and 3 shows that the observed photo-CIDNP effect inversion at long correlation times is due to the difference in the self-relaxation rates of the $L_{\pm} + 2L_{\pm}N_Z$ and $L_{\pm} - 2L_{\pm}N_Z$ eigenstates:

$$R_{L_{\pm} - 2L_{\pm}N_Z} - R_{L_{\pm} + 2L_{\pm}N_Z} = \frac{X_{G1,HFC}}{15} [4J(0) + 3J(\omega_L)] \quad (18)$$

This difference is plotted in Figure 9. Due to the presence of the $J(0)$ term in the spectral density part, this difference increases linearly as a function of the rotational correlation time and, at longer correlation times, quickly becomes large enough ($> 10^9$ s⁻¹) to be operational on the sub-microsecond geminate spin dynamics time scale.

Physically, the result above means that the two components of the ¹⁹F hyperfine doublet relax in the transverse plane at different rates; that is, electron L relaxes at different speeds for different nuclear configurations, which ultimately yields an electronic singlet or triplet that is conditional upon the nuclear spin state – similar in nature to the usual CIDNP generation scheme, but stemming from relaxation. These are pseudosecular transverse processes, which is why they were not picked up by the earlier models (some of which did include the secular transverse processes^{56,57}). When the radicals recombine, the

(50) Redfield, A. G. The Theory of Relaxation Processes. In *Advances in Magnetic Resonance*; Waugh, J. S., Ed.; Academic Press: New York, 1965; Vol. 1, pp 1–30.

(51) Wagner-Rundell, N. D.Phil. thesis, University of Oxford, 2007.

(52) Noyes, R. M. *J. Am. Chem. Soc.* **1956**, *78*, 5486–5490.

(53) Noyes, R. M. *J. Am. Chem. Soc.* **1955**, *77*, 2042–2045.

(54) Kaptein, R. *J. Am. Chem. Soc.* **1972**, *94*, 6262–6269.

(55) Kaptein, R. *J. Am. Chem. Soc.* **1972**, *94*, 6251–6262.

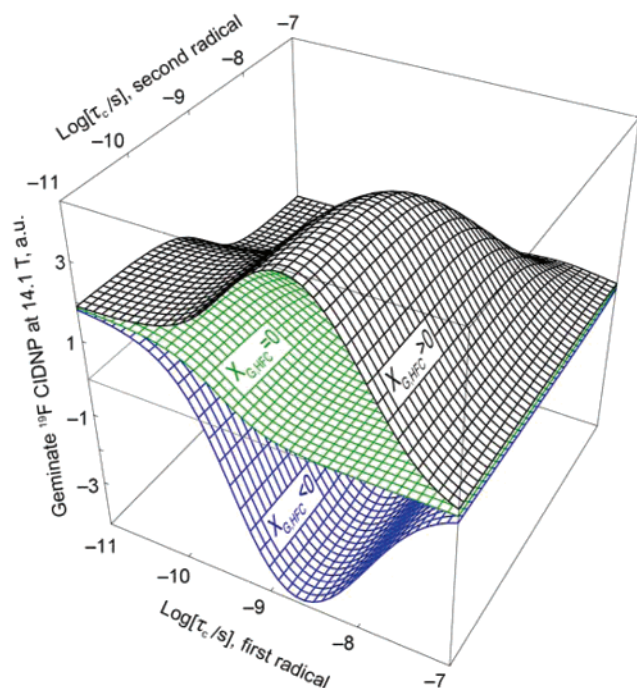


Figure 8. Rotational correlation-time dependence of the computed geminate ^{19}F photo-CIDNP effect in the 3-fluorotyrosine/FMN system at 14.1 T magnetic field. For the simulation details, see text.

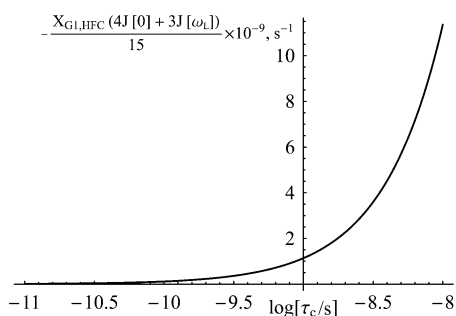


Figure 9. Rotational correlation-time dependence of the difference between the relaxation rates of $L_{\pm} + 2L_{\pm}N_z$ and $L_{\pm} - 2L_{\pm}N_z$ eigenstates in 3-fluorotyrosyl radical at 14.1 T using computed values of hyperfine and g -tensor anisotropy.

electron component disappears, leaving the correlation-time-dependent nuclear magnetization behind. This situation is qualitatively similar to that arising in ^1H - ^{15}N TROSY spectroscopy of large proteins, where the DD-CSA cross-correlation causes one signal in the ^{15}N doublet to relax much faster than the other in the transverse plane.⁵⁸ The situation that we have here is mathematically similar, although the frequency differences are, of course, much larger in an electron-nucleus system. The same cross-correlation is in part responsible for the line width variations sometimes observed in conventional EPR spectra: VO^{2+} , for example, shows eight hyperfine lines with widths that depend on the spin projection quantum number. The

$\Delta\text{HFC}-\Delta g$ cross-correlation is responsible for the linear term in this dependence.⁵⁹

Conclusions

We have described the experimental results and the theoretical models for relaxation processes occurring during fluorine-containing geminate radical pair evolution on a nanosecond time scale. At magnetic fields of over 10 T, electron-nucleus dipolar cross-relaxation (the Overhauser effect)^{11,17,18} and longitudinal $\Delta\text{HFC}-\Delta g$ (hyperfine anisotropy to g -tensor anisotropy) cross-correlation^{14–16,19} are shown to be negligibly slow. The dominant relaxation process is the transverse $\Delta\text{HFC}-\Delta g$ cross-correlation, which is shown to lead to an inversion in the geminate ^{19}F CIDNP phase for sufficiently large molecular tumbling rates. The essential feature of the spin dynamics model employed is the use of the complete spin state space and the complete relaxation superoperator. On the basis of the results above, we recommend this approach for reliable treatment of magnetokinetic systems in which relaxation effects are important.

Beyond its conceptual value, the correlation-time dependence of the geminate ^{19}F photo-CIDNP effect does have practical uses, as it provides a direct measure of the rotational correlation time in short-lived radical species. In particular, using the equations reported above, the fluorine-labeled tyrosine and tryptophan amino acids may be used as quantitative probes of side-chain correlation time in proteins,⁹ along with the use of photo-CIDNP effects as solvent accessibility probes.⁸ Apart from the fluorinated radicals, the results are likely to be applicable to ^{13}C - and ^{15}N -containing radicals, as these nuclei can also have rather large isotropic and anisotropic HFCs in aromatic radicals. Another interesting question, in the context of the unexplained CIDEP patterns recently discussed by Borbat et al.,^{36,60} is whether the complete relaxation matrix treatment also predicts those CIDEP effects and which relaxation pathways are responsible. More generally, because it is now possible to do brute force analytical relaxation theory on nontrivial spin systems,²⁶ it seems worthwhile to embark on a deeper general investigation into relaxation-driven radical spin dynamics.

Acknowledgment. We thank the Oxford Supercomputing Centre for the generous allocation of CPU time and Dr. Ken Hun Mok for enlightening discussions. We are indebted to Prof. Niels Andersen and Dr. Jasper Lin (University of Washington) for the gift of TC5b and for assistance with the preparation of its ^{19}F -labeled form (supported by NIH grant GM059658). I.K. is a Fellow by Examination at Magdalen College, Oxford. This work was supported in part by the BBSRC.

Supporting Information Available: Complete ref 24; source code for the program used to perform the simulations described in the text, Gaussian03 logs of the DFT calculations, and source code for the hyperfine tensor plotting program (in a ZIP-compressed file). This material is available free of charge via the Internet at <http://pubs.acs.org>.

JA0705792

(56) Den Hollander, J. A.; Kaptein, R. *Chem. Phys. Lett.* **1976**, *41*, 257–263.
 (57) Evans, G. T.; Fleming, P. D., III; Lawler, R. G. *J. Chem. Phys.* **1973**, *58*, 2071–2078.
 (58) Pervushin, K.; Riek, R.; Wider, G.; Wüthrich, K. *Proc. Natl. Acad. Sci. U.S.A.* **1997**, *94*, 12366–12371.

(59) Carrington, A.; McLachlan, A. D. *Introduction to magnetic resonance: with applications to chemistry and chemical physics*; Harper and Row: New York, 1967.
 (60) Borbat, P. P.; Milov, A. D.; Molin, Y. N. *Chem. Phys. Lett.* **1989**, *164*, 330–334.